Available online at www.sciencedirect.com
ScienceDirect
Tetrahedron
Tetrahedron 63 (2007) 12007–12014

Role of positional isomers on receptor–anion binding and evidence for resonance energy transfer

D. Amilan Jose,[a] D. Krishna Kumar,[a] Prasenjit Kar,[a] Sandeep Verma,[b] Amrita Ghosh,[a] Bishwajit Ganguly,[a,*] Hirendra N. Ghosh[b,*] and Amitava Das[a,*]

[a]*Central Salt and Marine Chemicals Research Institute (CSIR), Bhavnagar 364002, India*
[b]*Radiation and Photochemistry Division, Bhabha Atomic Research Center, Bombay, India*

Received 3 May 2007; revised 16 August 2007; accepted 6 September 2007
Available online 11 September 2007

Abstract—New urea-based sensors show a strong affinity for F^-, CH_3COO^-, and $H_2PO_4^-$ with an appreciable color change in the presence of excess F^-. The position of the nitro group in the urea derivative influences the relative affinity toward anionic analytes. Spectral and ab initio studies showed the difference in the deprotonation sites for the *ortho*- and *meta*/*para*-isomers in these cases. Photophysical studies confirmed the resonance energy transfer in the case of the *ortho*-isomer. The *ortho*-isomer can act as a dual emission probe for F^-.

1. Introduction

Anions, namely F^-, CH_3COO^-, and $H_2PO_4^-$, play a major role in many biological processes[1] and are involved in agricultural fertilizers as well as in food additives. Such anions have deleterious effects on the environment.[2] Thus, the search for a chemosensor that recognizes and detects these anionic analytes has emerged as a research area of considerable importance.[3] A selective sensor molecule should essentially have a receptor component specific for a selected analyte and a signaling unit capable of translating the analyte-binding induced changes into an output signal. This change in output signal is generally probed either through spectroscopy (e.g., fluorescence,[4] electronic, and NMR[5,6]) or by evaluating a redox potential. In this regard, colorimetric sensors have a definite advantage for recognizing an anionic analyte by visual color change.[3,5] There are many urea-based receptor molecules available in the literature, which act as a colorimetric sensor for F^-.[7] The visual color change on F^- ion binding arises due to the more favored intramolecular charge transfer (ICT) process in the receptor·F^- adduct as compared to the receptor molecule alone.[8] These receptors derivatized with electron withdrawing functionality can lead to Bronsted acid–base equilibrium in presence of excess F^-. The high thermodynamic stability of HF_2^- governs the acid–base equilibrium process.[9] However, studies to elucidate the influence of the positional isomers (electron withdrawing substituents) on the acidity and ICT are lacking in the literature. Therefore, this prompted us to examine the influence of positional isomers of nitro-substituents on the intramolecular charge transfer with a suitable receptor molecule.

In this paper, we report dissymmetric deprotonation of three new isomeric sensor molecules (**L_1–L_3**, Scheme 1) with associated color change in the presence of excess F^- (>2 equiv). All three isomers **L_1–L_3** associate strongly to F^- ($[F^-]\leq 1.2$ equiv) and get deprotonated in the presence of excess F^- (>2 equiv). However, the sites of deprotonation varied for these receptors. It has been found that **L_1–L_3** also showed strong association with CH_3COO^- and $H_2PO_4^-$ as well. The position of the nitro functionality in these

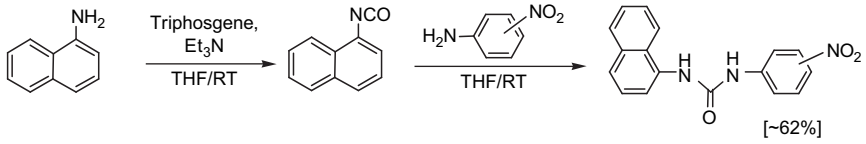

Scheme 1. Synthesis of receptors **L_1–L_3**. 1-Naphthalen-1-yl-3-(2-nitro-phenyl)-urea=**L_1**; 1-naphthalen-1-yl-3-(3-nitro-phenyl)-urea=**L_2**; 1-naphthalen-1-yl-3-(4-nitro-phenyl)-urea=**L_3**.

* Corresponding authors. Tel.: +91 278 256 7760; fax: +91 278 256 7562; e-mail addresses: hnghosh@barc.gov.in; ganguly@csmcri.org; amitava@csmcri.org

0040–4020/$ - see front matter © 2007 Elsevier Ltd. All rights reserved.
doi:10.1016/j.tet.2007.09.008

derivatives is found to influence the acidity of the N–H protons in the urea functionality and thereby the affinity of respective receptors toward analytes. These observations were rationalized at RHF/6-31G* calculations. Further, photophysical studies resolved the resonance energy transfer in the case of the *ortho*-isomer (**L_1**).

2. Results and discussion

A one-step synthesis of the new chromogenic sensor molecules **L_1**–**L_3** was achieved (Scheme 1) in good yield. All these receptor molecules were characterized using standard analytical and spectroscopic techniques.

The single crystal X-ray structure of **L_3** was obtained from DMSO solution (Fig. 1a) in a centrosymmetric monoclinic space group $P2_1/c$. The asymmetric unit comprises one ligand and a solvent DMSO molecule. One of the oxygen atoms of the nitro group displays non-bonded interaction with the solvated DMSO molecule through C–H···O interaction. These two interactions result in a zero-dimensional hydrogen bonded macrocycle in which two ligands and two DMSO are involved (Fig. 1b and Supplementary data).

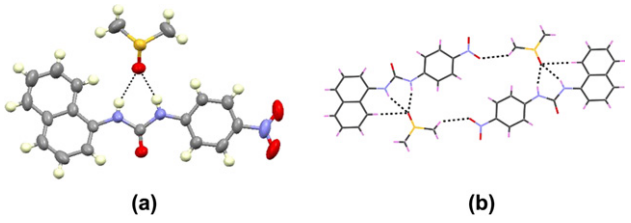

Figure 1. (a) Thermal ellipsoidal plot (50% probability) of compound **L_3**; (b) Illustration of various hydrogen bonding interactions resulting in zero-dimensional hydrogen bonding network.

Preliminary studies revealed that dilute solutions ($\sim 10^{-5}$ M) of **L_1**–**L_3** were very pale yellow in color, which changed to orange upon addition of excess *n*-Bu_4NF and could be detected visually and spectrophotometrically (Figs. 2 and 3). No such color change was observed for CH_3COO^- or $H_2PO_4^-$ ions, however, electronic and fluorescence spectral changes were registered (Figs. 3 and 4 and Supplementary data Figs. 4–8). The change in the luminescence and electronic spectral pattern for **L_1**, **L_2**, and **L_3** (λ_{ext}=288 nm) on addition of 1–1.2 equiv of F^-, CH_3COO^-, or $H_2PO_4^-$ revealed the binding of these analytes with the urea receptor unit. No significant change was detected visually or in electronic/luminescence spectra in presence of other tetrabutylammonium salts of Cl^-, Br^-, I^-, NO_2^-, or HSO_4^-. However, the possibility of weak binding of these anions to the receptors cannot be excluded as indicated by ^{1}H NMR studies (Supplementary data Figs. 8 and 9). Change in the electronic and emission spectral pattern on addition of increasing [F^-] revealed a distinct difference between **L_1** and **L_2**/**L_3**, shown in Figure 4. For spectrophotometric titration up to 1.2 equiv of F^-, isosbestic points appeared at 412, 354, and 353 nm for **L_1**, **L_2**, and **L_3**, respectively (Fig. 4a–c), but no color change was detected by the naked eye.

Further, addition of F^- (1.8–10 equiv, 3.6×10^{-5}–2.0×10^{-4} M) caused a distinct color change from pale yellow to orange in all three cases. A new absorption band at 467 nm (new isosbestic points at 354 and 409 nm) was noticed for **L_2**. A similar band also appeared for **L_3** at 465 nm (new isosbestic points at 353 and 405 nm). On the other hand, for **L_1** an increase in the absorbance at 325–355 nm and 450–520 nm was observed with the eventual appearance of a broad absorption band at 476 nm with a new isosbestic point at 412 nm. The newly developed absorption band for **L_1**, **L_2**, and **L_3** in the visible region was due to the intramolecular charge transfer (ICT) transition between the deprotonated urea units and the electron deficient

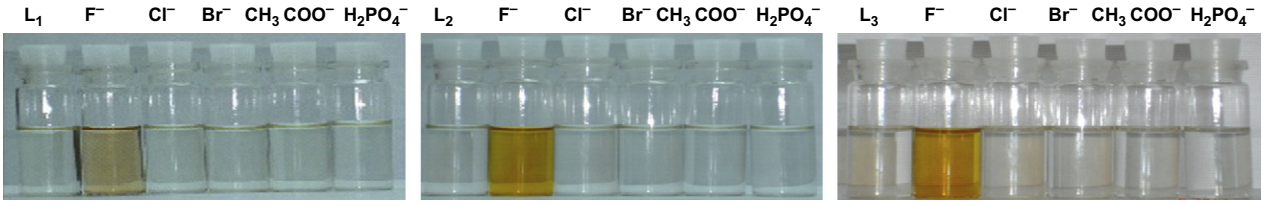

Figure 2. Color changes of receptors **L_1**, **L_2**, and **L_3** at rt (2×10^{-5}) with different anions (6×10^{-5}) in DMSO/CH_3CN (1:9, v/v).

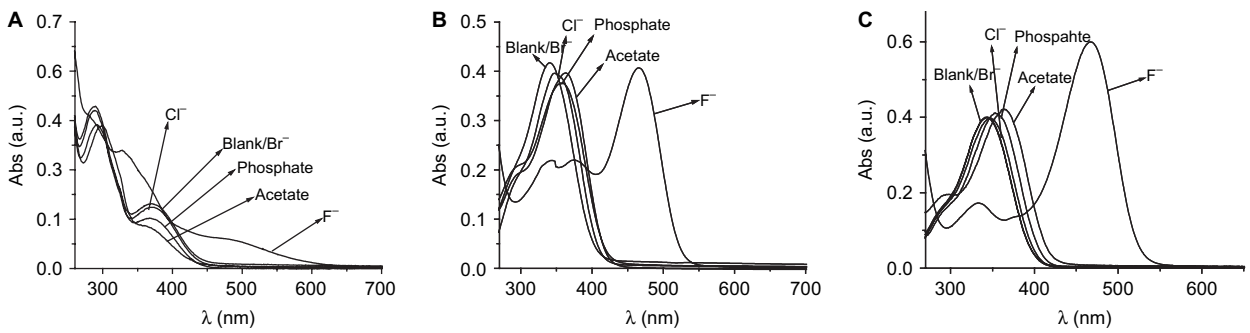

Figure 3. UV–vis changes of receptor **L_1** (A); **L_2** (B); and **L_3** (C) at rt (2×10^{-5}) with different anions in DMSO/CH_3CN (1:9, v/v) mixture.

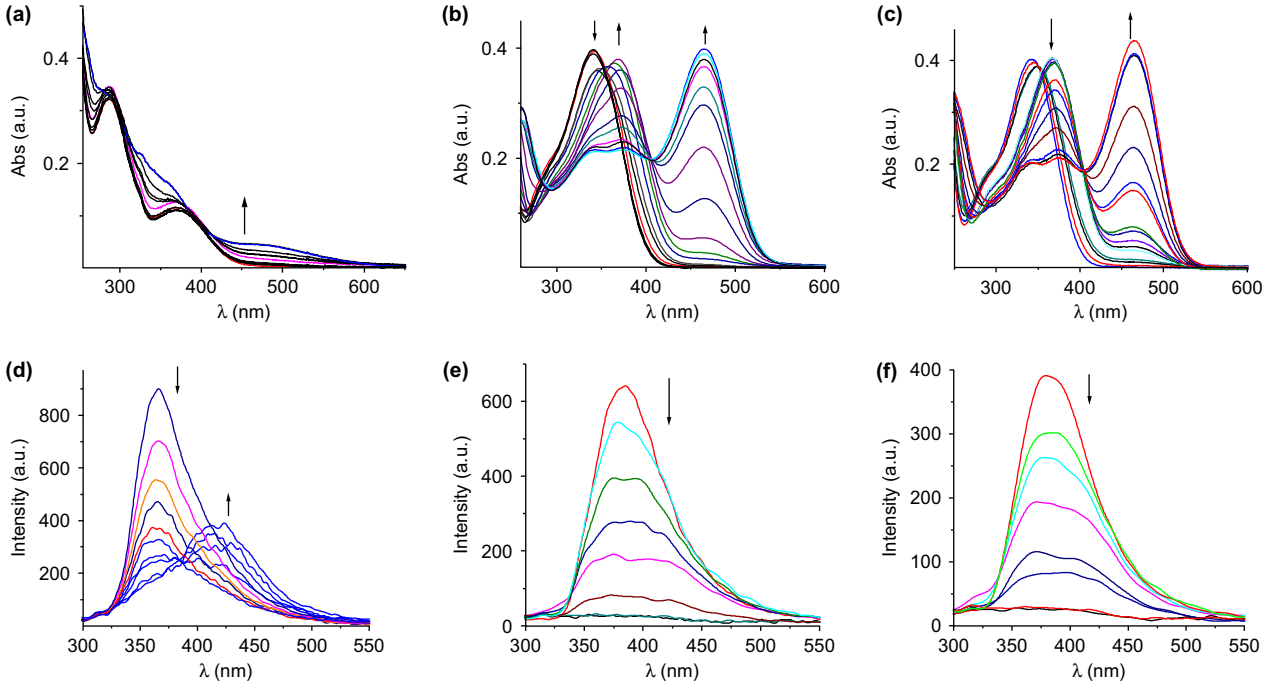

Figure 4. Change in electronic (a–c) and emission spectra (d–f) for 2.0×10^{-5} M [in 1:9 (v/v) DMSO/CH_3CN] of $\mathbf{L_1}$ (a and d); $\mathbf{L_2}$ (b and e); $\mathbf{L_3}$ (c and f) on addition of varying [*n*-Bu_4NF] (5.0×10^{-6}–2.0×10^{-4} M).

nitrobenzene moiety. A similar color change was also reported for the symmetric bis-*para*-nitrobenzyl urea in the presence of excess F^- and concluded to be an ICT transition.[9a] The titration profile obtained for $\mathbf{L_1}$, $\mathbf{L_2}$, and $\mathbf{L_3}$ from the spectrophotometric titration using F^- solution as titrant clearly showed the presence of two distinct equilibria. The first one was for the adduct formation (K_a; Eq. 1; LH represents the receptor molecule); whereas, the second one was for the Bronsted acid–base reaction (K_d; Eq. 2). A color change in the presence of *n*-Bu_4NOH was also obtained and similar observations were also reported.[8c] No further change in the spectral pattern was observed on addition of a large excess of F^- (100 equiv). Thus, the second deprotonation of the urea moiety did not take place in the present study.[9a] Equilibrium constants for adduct formation and proton dissociation are shown in Table 1.

However, electronic spectral studies did not give any indication about the site of deprotonation in $\mathbf{L_1}$, $\mathbf{L_2}$, and $\mathbf{L_3}$ and this was resolved with the help of ab initio calculations (vied infra) and emission spectral studies.

$$LH + F^- \rightleftarrows [LH\cdots F] \qquad K_a \tag{1}$$

$$[LH\cdots F]^- + F^- \rightleftarrows L^- + HF_2^- \quad K_d \tag{2}$$

Spectrophotometric titrations were also carried out for $\mathbf{L_1}$, $\mathbf{L_2}$, and $\mathbf{L_3}$ using Cl^-, CH_3COO^-, and $H_2PO_4^-$ as the anionic analytes. The titration profiles show that 1:1 adduct formation takes place in all cases. The calculated association constants and pertinent spectroscopic parameters are given in Table 1. The observed sequence of log *K* values for adduct formation (Eq. 1) was $F^- > CH_3COO^- > H_2PO_4^- \gg Cl^-$.

To examine the receptor–analyte interactions, the structures of $\mathbf{L_1}$–$\mathbf{L_3}$ and their corresponding adducts with various anions were optimized (Fig. 5) using RHF/6-31G* level of theory.[10] The calculated geometry for $\mathbf{L_1}$ revealed the presence of an intramolecular hydrogen bond (Fig. 5a). Structural parameters of $\mathbf{L_3}$ were found to agree with the single crystal X-ray data (Fig. 1). The results from RHF/6-31G* calculations show that $\mathbf{L_2}$ and $\mathbf{L_3}$ bind more strongly to F^- than $\mathbf{L_1}$ (Table 2). Single point calculations performed with RHF/6-31+G* using RHF/6-31G* optimized geometries showed similar trends in the binding energies (Table 2). As expected, calculations performed using an acetonitrile continuum solvent model exhibited lower binding energies than the corresponding gas phase calculations (Table 2).

More importantly, a similar binding trend for F^- was observed in the solvated system ($\mathbf{L_2}$ and $\mathbf{L_3} > \mathbf{L_1}$). The affinity constant values, measured experimentally for the association of F^- with $\mathbf{L_1}$–$\mathbf{L_3}$, suggested that $\mathbf{L_2}$ and $\mathbf{L_3}$ had higher

Table 1. Constant for the complex formation equilibrium[a]

	F^-	Cl^-	CH_3COO^-	$H_2PO_4^-$
log K_{1a}	3.01 (2)	—	2.90 (2)	2.64 (1)
log K_{1d}	4.77 (2)	—	—	—
log K_{2a}	3.67 (1)	1.79 (2)	3.03 (1)	2.70 (1)
log K_{2d}	4.96 (1)	—	—	—
log K_{3a}	3.83 (1)	1.42 (3)	3.34 (1)	3.28 (1)
log K_{3d}	5.04 (1)	—	—	—

[a] Tertiary butyl ammonium salts of the respective anions were used for the studies. The log *K* value reported (K_1, K_2, and K_3 values are for receptors $\mathbf{L_1}$, $\mathbf{L_2}$, and $\mathbf{L_3}$, respectively) is the average of the five independent data evaluated from each individual UV–vis titration data for the respective receptor and anion. The value provided in the parentheses is the uncertainty in the last digit.

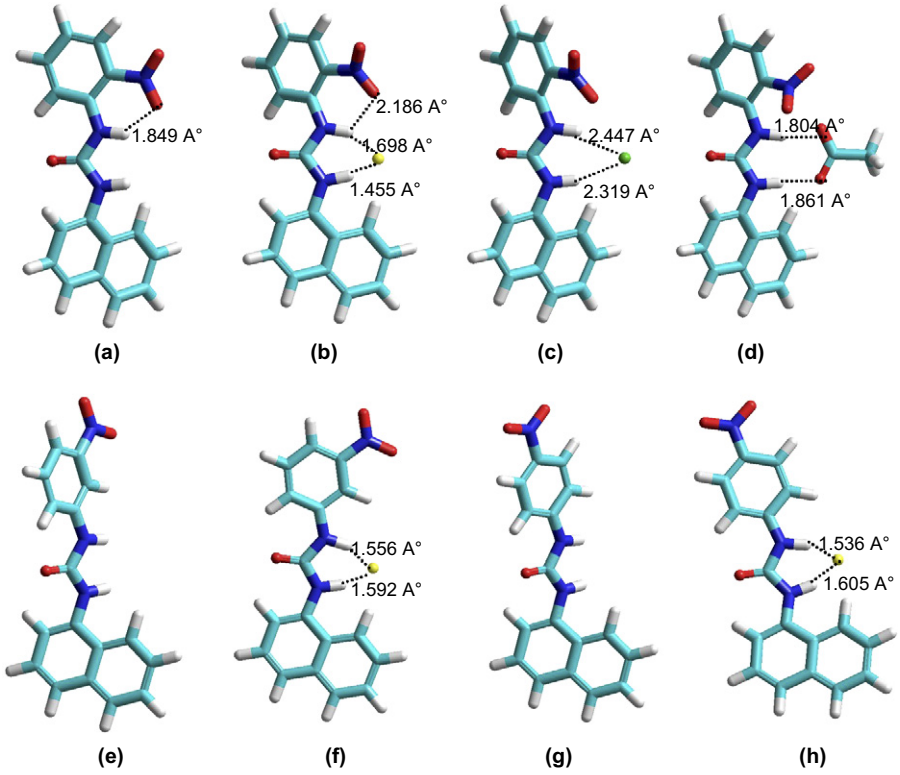

Figure 5. RHF/6-31G* optimized geometries for the free receptors and selected adducts: (a) $\mathbf{L_1}$; (b) $\mathbf{L_1}\cdot F^-$; (c) $\mathbf{L_1}\cdot Cl^-$; (d) $\mathbf{L_1}\cdot CH_3COO^-$; (e) $\mathbf{L_2}$; (f) $\mathbf{L_2}\cdot F^-$; (g) $\mathbf{L_3}$; (h) $\mathbf{L_3}\cdot F^-$. Color code: red=oxygen; dark blue=nitrogen; gray=hydrogen; yellow=fluoride.

affinity for F^- than $\mathbf{L_1}$. This agrees well with the above calculations (Table 1). The observed sequence of log K values for adduct formation (Eq. 1) was $F^->CH_3COO^->H_2PO_4^-$. These results suggest that the acetate and phosphate ions have lower affinities than the F^- ion. To examine this trend, we have calculated the relative binding energies of F^-, Cl^-, CH_3COO^-, and $H_2PO_4^-$ with $\mathbf{L_1}$. The calculated binding energies in the gas phase for $\mathbf{L_1}$ indeed showed higher affinity toward F^- ion (Supplementary data Table 4). The binding trend remains the same in acetonitrile solution. Closer examination of the optimized structures for $\mathbf{L}_n\cdot F^-$ (n=1, 2, or 3) revealed that N–H···F hydrogen bonds are asymmetric in nature in all cases (Fig. 5). The N–H···F^- hydrogen bond for the N–H bond adjacent to the electron withdrawing nitrobenzene unit was found to be shorter relative to the N–H bond adjacent to the naphthalene ring in $\mathbf{L_2}$ and $\mathbf{L_3}$. As a result, deprotonation is expected to occur from the N–H adjacent to the nitrobenzene unit for these two receptors. However, the reverse holds true in the case of $\mathbf{L_1}$ (Fig. 5b). Intramolecular hydrogen bonding prevents deprotonation of the N–H hydrogen adjacent to the nitrobenzene unit.

The calculated Y-type interaction[8c] of acetate with $\mathbf{L_1}$ receptor was supported by the single crystal obtained for $\mathbf{L_3\cdot CH_3COO^-}$, which was grown from a mixed CH_3CN/DMF solution (~9:1, v/v). The X-ray structure for $\mathbf{L_3\cdot CH_3COO^-}$ crystallized in a centrosymmetric monoclinic space group $P2_1/c$ is shown in Figure 6. The asymmetric unit comprises the ligand and tetrabutylammonium acetate (Supplementary data Fig. 3).

Steady state luminescence spectra (Fig. 4d–f) show that $\mathbf{L_1}$, $\mathbf{L_2}$, and $\mathbf{L_3}$ give an emission band at ~365 nm upon excitation of the naphthalene unit at 280 nm. Quantum yields were found to be similar in all cases. However, the emission spectral pattern varies in presence of F^-. For $\mathbf{L_2}$ and $\mathbf{L_3}$, emission quantum yields were found to decrease monotonically with an increase in [F^-] (Figs. 4e and 3f).

Table 2. Calculated interaction energies for receptor·F^- complexes in kcal/mol[a]

Basis set	$\mathbf{L_1}\cdot F^-$	$\mathbf{L_2}\cdot F^-$	$\mathbf{L_3}\cdot F^-$
RHF/6-31G*	−78.3 (−21.7)	−91.3 (−25.3)	−95.2 (−26.2)
RHF/6-31+G*	−49.2 (−10.3)	−62.7 (−22.3)	−66.5 (−22.6)

[a] Energies calculated in acetonitrile are given in parentheses.

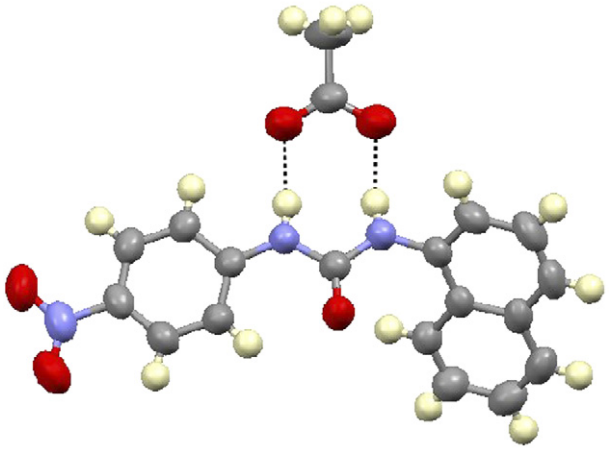

Figure 6. Thermal ellipsoidal plot (50% probability) of compound $\mathbf{L_3\cdot CH_3COO^-}$ $(n\text{-Bu})_4N$, TBA cation is omitted for clarity.

For $\mathbf{L_1}$, the situation was quite different (Fig. 4d). In this case, changes in the luminescence intensity for the naphthalene based fragment (with λ_{ext}=288 nm) was found to decrease with increasing [F^-], until 1.2 mol equiv were added. Upon addition of further F^-, a growth in the emission intensity was registered at 417 nm along with a simultaneous decrease in emission intensity at 366 nm (Supplementary data Fig. 9). Appearance of a new isoemissive point at 386 nm clearly suggested a new equilibrium process corresponding to the acid–base reaction (Eq. 2).[11]

The position of this new broad emission band at 417 nm remained unaffected with changes in solvent polarity. A separate study confirmed that the band at 417 nm is due to nitrobenzene emission (Supplementary data Fig. 12). It is to be noted that this emission band is completely absent in the pure *ortho*-isomer. We have attributed this observation to the fluorescence resonance energy transfer (FRET) from the photo-excited naphthalene moiety to the nitrobenzene moiety in the *ortho*-isomer. To corroborate this presumption, we have performed time-resolved emission studies for these receptors in the absence and presence of F^-.

The time-resolved emission for the *ortho*-isomer ($\mathbf{L_1}$) was studied upon excitation at 308 nm. The emission decay

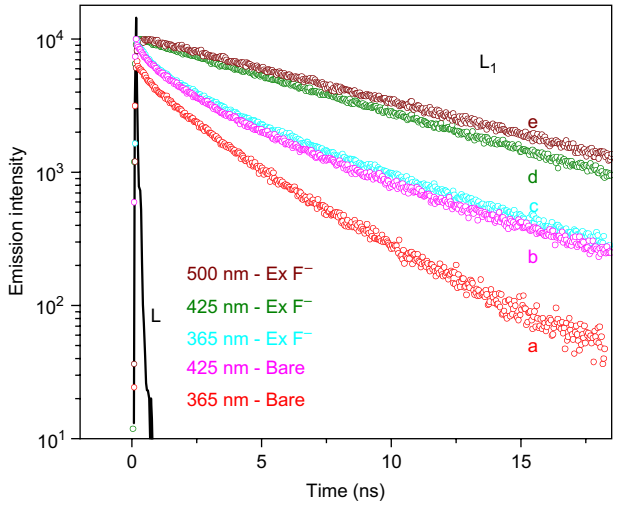

Figure 7. Single photon counting studies of $\mathbf{L_1}$ (25 μM) in DMSO/CH_3CN (1:9, v/v) mixture following excitation at 308 nm in the absence and presence of excess [F^-]: (a) λ_{em}=365 nm; (b) λ_{em}=425 nm; (c) with excess [F^-] (λ_{em}=365 nm); (d) with excess [F^-] (λ_{em}=425 nm); and (e) with excess [F^-] (λ_{em}=500 nm). **L** is the laser pulse.

profile monitored at 365 nm could be fitted multi-exponentially with three constants $\tau_1 \leq 10$ ps (37%), τ_2=1.75 ns (47.7%), and τ_3=6.2 ns (15.3%) (Fig. 7).

Among these, the 1.75 ns component could be attributed to the radiative lifetime of the naphthalene moiety, while the 6.2 ns component is the radiative lifetime of the nitrobenzene moiety. However, the faster decay component (<10 ps) might not be due to any real emissive species. Both of these NH groups are expected to form weak intermolecular H-bonding with the bulk solvent. As a result, on photo-excitation, extra energy could be tunneled through to the bulk by a non-radiative pathway. These kinds of decay dynamics are generally very fast and non-exponential in nature.[12] Similarly, a non-exponential fast decay component was also observed, when the emission decay profile was monitored at other wavelengths (Table 3). The time-resolved emission studies of $\mathbf{L_1}$ in the presence of the fluoride ion were also studied upon excitation at 308 nm. The emission decay was monitored at three different wavelengths 365, 425, and 500 nm (Table 3). It was observed that at 500 nm the emission decay was a single exponential with a single component of 8.7 ns, which could be attributed to the decay of the emission of the pure nitrobenzene fragment. However, when emission was monitored at 425 and 365 nm, the decay profile could be fitted bi- and tri-exponentially, respectively, in the presence of excess [F^-]. It was very interesting to see that with increasing fluoride concentration the contribution of the fast decay component (<10 ps) was found to decrease drastically. Again emission decay kinetics monitored at 365 nm in the presence of excess [F^-] has all three decay components. However, kinetics at a monitoring wavelength of 425 nm has only two decay components, which correspond to the discrete naphthalene and nitrobenzene moieties.

Importantly, at a red monitoring wavelength (500 nm), emission due to the naphthalene fragment is completely absent. Presumably, in the presence of excess [F^-], $\mathbf{L_1}$ exists in the mono-deprotonated form ($\mathbf{L_1}$-H) due to the deprotonation of the NH group adjacent to the naphthalene moiety and the other intramolecularly bound urea (N–H) functionality is preferentially bound to F^- through a H-bond, rather than to the bulk solvent molecule(s). This is expected to minimize or exclude the possibility of intermolecular H-bonding with solvent molecules and thereby the possibility of de-excitation following the non-radiative channel and eventually energy transfer takes place from the naphthalene moiety to the nitrobenzene moiety.

Table 3. Emission life times of $\mathbf{L_1}$ in DMSO/CH_3CN (1:9, v/v) mixture following excitation at 308 nm at various monitoring wavelengths in the absence and presence of varying [F^-]

Monitoring wavelength	$\mathbf{L_1}$	$\mathbf{L_1}$ with F^- (1:1)	$\mathbf{L_1}$ with F^- (excess)
365 nm	τ_1=0.010 ns (37%) τ_2=1.75 ns (47.7%) τ_3=6.2 ns (15.3%)	τ_1=0.010 ns (30%) τ_2=1.76 ns (57.9%) τ_3=6.14 ns (12.1%)	τ_1=0.009 ns (6.2%) τ_2=1.53 ns (77.8%) τ_3=6.62 ns (16%)
425 nm	τ_1=0.009 ns (10.7%) τ_2=1.741 ns (69%) τ_3=6.790 ns (20.3%)	τ_1=Absent τ_2=1.467 ns (22%) τ_3=5.98 ns (78%)	τ_1=Absent τ_2=1.42 ns (6%) τ_3=7.48 ns (94%)
500 nm		τ_1=Absent τ_2=1.7 ns (11.6%) τ_3=8.24 ns (88.4%)	τ_1=Absent τ_2=Absent τ_3=8.732 ns (100%)

Thus, time-resolved studies clearly demonstrate that in the presence of F^-, resonance energy transfer from the naphthalene moiety to the nitrobenzene moiety was favored. Further, the time-resolved emission studies did not show these features for $\mathbf{L_2}$ and $\mathbf{L_3}$, when studied under similar conditions (Supplementary data Fig. 13).

3. Conclusion

In summary, we have demonstrated that receptors $\mathbf{L_1}$–$\mathbf{L_3}$ effectively bind F^-, CH_3COO^-, and $H_2PO_4^-$ over other anions used in this study. Furthermore, these receptors can act as colorimetric sensors for fluoride ions through deprotonation of the urea moiety in the presence of $[F^-]>2.0$ equiv. The computed ab initio results rationalized the relative affinity of these positional isomers toward the anions studied herein and suggested different deprotonation sites in the $\mathbf{L_1}$ versus $\mathbf{L_2}$/$\mathbf{L_3}$ receptors. The importance of positional isomers of electron withdrawing substituents was further established by time-resolved emission studies. The resonance energy transfer is possible only for the *ortho*-isomer ($\mathbf{L_1}$) and this receptor molecule was found to act as a dual emission probe for F^-.

4. Experimental section

4.1. Materials and methods

1-Amino naphthalene, 1-isocyanato-4-nitrobenzene, and triphosgene were obtained from Aldrich. 2-Nitroaniline, 3-nitroaniline, 4-nitroaniline, and triethylamine were obtained from S.D Fine chemicals (India). All other chemicals were obtained locally and used as such, unless otherwise stated. Solvents for reactions and various studies were used as received from Merck (India)—except THF and DMF, which were dried prior to the use of the following standard methods. Microanalyses (C, H, N) were performed using a Perkin Elmer 4100 elemental analyzer. FTIR spectra were recorded as KBr pellets using a Perkin Elmer Spectra GX 2000 spectrometer. ^{1}H NMR spectra were recorded on a Bruker 200 MHz FT NMR (model: Avance-DPX 200) using CD_3CN as the solvent and tetramethylsilane (TMS) as an internal standard. Electronic spectra were recorded with a Shimadzu UV-3101 PC spectrophotometer, while room temperature luminescence spectra were recorded with a Perkin Elmer LS 50B luminescence spectrofluorimeter, fitted with a red sensitive photo multiplier. Ferrocene was added at the end of each experiment as the internal standard and all potentials are quoted versus the ferrocene/ferrocenium (Fc/Fc^+) couple. ESI MS measurements were carried out on Waters Qtof-Micro instrument.

4.2. Crystallographic details

Crystal data for $\mathbf{L_3}$ and $\mathbf{L_3}\cdot\mathbf{CH_3COO^-}$ were collected using Mo Kα (λ=0.7107 Å) radiation on a SMART APEX diffractometer equipped with a CCD area detector at 100 K. Crystals were selected from the mother liquor and immersed in Partone oil and then mounted. Data collection, data reduction, structure solution/refinement were carried out using the software package of SMART APEX.[13] Graphics were generated using MERCURY 1.4.[14] Empirical absorption corrections were performed using equivalent reflections with the program SADABS. Both the structures were solved by direct methods. In $\mathbf{L_3}\cdot\mathbf{CH_3COO^-}$ the carbon atoms of the tetrabutylammonium salt were found to be disordered and were modeled using the SADI and DFIX instruction in SHELXL.[15] All hydrogen atoms were geometrically fixed at their idealized position.

Crystallographic data for the structural analysis of compounds reported herein have been deposited at the Cambridge Crystallographic Data Center, CCDC no. 616327–616328. Copies of this information may be obtained free of charge from The Director, CCDC, 12 Union Road, Cambridge, CB2 1EZ, UK (fax: +44 1233 336 033; e-mail: deposit@ccdc.cam.ac.uk or http://www.ccdc.cam.ac.uk). Crystallographic parameters are listed in Supplementary data Table 2.

4.3. Spectrophotometric titrations

A solution (1.0×10^{-4} M) of the compounds $\mathbf{L_1}$, $\mathbf{L_2}$, and $\mathbf{L_3}$ in DMSO/acetonitrile (1:9, v/v) was prepared and stored in the dark. These solutions were used for all spectroscopic studies after appropriate dilution. A solution (1.0×10^{-3} M) of tetrabutylammonium salts of the respective anions was prepared in dried and distilled acetonitrile, prior to use and were stored under an inert atmosphere. All titration experiments were performed using 2.0×10^{-5} M solutions of complexes $\mathbf{L_1}$, $\mathbf{L_2}$, and $\mathbf{L_3}$ in DMSO/acetonitrile (1:9, v/v) and various concentrations of anions (2.0×10^{-6}–1.0×10^{-4} M) in a DMSO/acetonitrile (1:9, v/v) mixture. Affinity constants were evaluated after calculating the concentrations of the respective species such as free $\mathbf{L_1}$, $\mathbf{L_2}$, $\mathbf{L_3}$, F^-, CH_3COO^-, $H_2PO_4^-$, and associated complexes, e.g., $\mathbf{L_1}\cdot F^-$, $\mathbf{L_2}\cdot F^-$, $\mathbf{L_3}\cdot F^-$.

4.4. Luminescence titrations

Standard solutions mentioned above were used for spectrophotometric titration and luminescence titration studies. For all measurements, λ_{ext} used was 288 nm with an excitation and emission slit width of 6 nm. All titration experiments were performed using a solution (2.5×10^{-5} M) of compounds $\mathbf{L_1}$, $\mathbf{L_2}$, and $\mathbf{L_3}$ in DMSO/acetonitrile (1:9, v/v) (thoroughly degassed before measurement with IOLAR grade dinitrogen gas saturated with acetonitrile vapor) and solutions of various anions (2.0×10^{-6}–5.0×10^{-3} M) in DMSO/acetonitrile (1:9, v/v).

4.5. Picosecond time-resolved fluorescence studies

Fluorescence lifetime measurements were carried out using a time-resolved fluorescence measurement setup and details of the system have been described elsewhere.[16] The only modification that has been carried out to the earlier system is the replacement of the pump laser with a newer one, which is Spectra Physics (Vanguard) cw mode-locked Nd:YAG (yttrium aluminum garnet) laser with a repetition rate of 80 MHz. The frequency-doubled and attenuated (from 2 to 0.6 W) output of the laser was used to pump the dye laser. The samples were excited at 308 nm, which is the frequency doubling of the dye laser output at 616 nm, and monitored at

different wavelengths. For fluorescence decay measurements, 10,000 peak counts were collected in 512 channels with a time increment of 40 ps/channel and each measurement was repeated three times. The measured fluorescence decays were analyzed using the iterative reconvolution method with the aid of the Marquardt algorithm as described by Bevington.[17] The criteria for a good fit were judged by statistical parameters such as the reduced χ^2 being close to unity and the random distribution of the weighted residuals.

4.6. Synthesis

4.6.1. Synthesis of 1-naphthalen-1-yl-3-(2-nitro-phenyl)-urea (L_1). To a stirred dry THF solution (80 ml) of 1-amino naphthalene (1.0 g, 6.99 mmol) and triethylamine (2 ml, 14 mmol), triphosgene (1.84 g, 6.2 mmol) dissolved in 20 ml of dry THF was added slowly to this solution under nitrogen atmosphere at ice-cooled condition. The mixture was allowed to stir at room temperature. After 30 min, 2-nitro aniline (0.964 g, 6.99 mmol) dissolved in 40 ml of dry THF was added to this reaction mixture. The reaction mixture was stirred at room temperature for one day and filtered. The solid obtained was washed with methanol and water. The desired compound was isolated as a yellow solid (1.15 g, 60%). ^{1}H NMR (200 MHz, DMSO-d_6) d (ppm): 9.790 (s, 1H, –NH), 9.710 (s, 1H, –NH), 8.256 (d, 1H, H^A, J=8.4 Hz), 8.15 (d, 1H, J=7.6 Hz), 8.096 (t, 1H, J=8.2 Hz), 7.932 (d, 1H, J=6 Hz), 7.818 (d, 1H, J=7.6 Hz), 7.73–7.68 (m, 2H), 7.56 (m, 3H), 7.21 (t, 1H, J=7.8 Hz). ^{13}C NMR (DMSO-d_6) δ (ppm): 153.1, 138.4, 135.0, 134.8, 133.9, 133.7, 128.5, 127.4, 126.3, 126.1, 125.9, 125.5, 124.7, 123.2, 124.6, 123.2, 122.7, 122.3, 120.3. FTIR (KBr; cm^{-1}): 3329 (NH), 3272 (NH), 1651 (–C═O). ESI MS [m/z (positive ion mode)]: 329.5 (M+Na$^+$, 40%). Elemental analysis for $C_{17}H_{13}N_3O_3$: calculated: C, 66.44; H, 4.26; N, 13.67. Found: C, 66.21; H, 4.20; N, 13.61.

4.6.2. Synthesis of 1-naphthalen-1-yl-3-(3-nitro-phenyl)-urea (L_2). The methodology adopted for the synthesis of receptor L_2 was the same as that mentioned for L_1. Instead of 2-nitro aniline, here 3-nitroaniline was used. Yield (1.15 g, ~62%). ^{1}H NMR (200 MHz, DMSO-d_6) d (ppm): 9.799 (s, 1H, –NH), 9.002 (s, 1H, –NH), 8.248 (d, 2H, J=9.2 Hz), 8.148 (d, 1H), 7.987 (d, 2H), 7.774 (d, 2H, J=9.2 Hz), 7.627–7.469 (m, 4H). ^{13}C NMR (DMSO-d_6) δ (ppm): 152.9, 148.2, 141.1, 133.8, 130.1, 128.4, 125.9, 125.8, 125.8, 124.2, 123.2, 126.4, 121.4, 118.4, 116.3, 112.0. FTIR (KBr; cm^{-1}): 3295 (NH), 1644 (–C═O). ESI MS [m/z (positive ion mode)]: 330.3 (M+Na$^+$, 20%). Elemental analysis for $C_{17}H_{13}N_3O_3$: calculated: C, 66.44; H, 4.26; N, 13.67. Found: C, 66.31; H, 4.34; N, 13.73.

4.6.3. Synthesis of 1-naphthalen-1-yl-3-(4-nitro-phenyl)-urea (L_3). Receptor L_3 was also synthesized by the same procedure explained above by using 4-nitroaniline. Yield (61%). ^{1}H NMR (200 MHz, DMSO-d_6) d (ppm): 9.762 (s, 1H, –NH), 8.981 (s, 1H, –NH), 8.19 (d, 2H, J=9.0 Hz), 8.072 (d, 1H, J=8.2 Hz), 7.93 (d, 2H, J=7.0 Hz), 7.92 (d, 1H, J=7.2 Hz), 7.71 (d, 2H, J=9.0 Hz), 7.70–7.67 (m, 1H), 7.59–7.44 (m, 2H). ^{13}C NMR (DMSO-d_6) δ (ppm): 152.5, 146.51, 140.1, 133.6, 133.4, 133.0, 126.3, 126.2, 126.0, 125.9, 125.6, 125.7, 125.1, 124.9, 123.9, 121.6, 121.2, 120.0, 118.6, 117.6, 117.2. FTIR (KBr; cm^{-1}): 3360 (NH), 3337 (NH), 1697 (–C═O). ESI MS [m/z (positive ion mode)]: 330.1 (M+Na$^+$, 100%). Elemental analysis for $C_{17}H_{13}N_3O_3$: calculated: C, 66.44; H, 4.26; N, 13.67. Found: C, 66.40; H, 4.21; N, 13.61. L_3 was also synthesized by following another methodology (Supplementary data). In both the methods, the yield was the same.

Acknowledgements

The Department of Science and Technology (DST) and the Board of Research in Nuclear Science (BRNS), Government of India, supported this work. Authors D.A.J. and D.K.K. wish to acknowledge CSIR for Sr. Research Fellowship. A.D., B.G., and H.N.G. wish to thank Dr. P. K. Ghosh (CSMCRI, Bhavnagar) and Dr. T. Mukherjee (BARC, Mumbai) for their keen interest in this work.

Supplementary data

Crystal data for receptor L_3 and $L_3 \cdot CH_3COO^-$ (CCDC 616327 and 616328), UV–vis, emission and ^{1}H NMR titration spectra, job plots, and final co-ordinates of the optimized structures are available free of charge via the internet. Supplementary data associated with this article can be found in the online version, at doi:10.1016/j.tet.2007.09.008.

References and notes

1. (a) *Ullman's Encyclopedia of Industrial Chemistry*, 6th ed.; Wiley-VCH: New York, NY, Germany, 1998; (b) Krik, K. L. *Biochemistry of Halogens and Inorganic Halides*; Plenum: New York, NY, 1991; p 59l.
2. (a) Rurack, K.; Resch-Genger, U. *Chem. Soc. Rev.* **2002**, *31*, 116–127; (b) Tajc, S. G.; Miller, B. L. *J. Am. Chem. Soc.* **2006**, *128*, 2532–2533.
3. For an overview on anion sensors please see following articles: (a) *Supramolecular Chemistry of Anions*; Bianchi, E., Bowman-James, K., Garcia-Espana, E., Eds.; Wiley-VCH: New York, NY, 1997; (b) Gale, P. A. Amide and Urea Based Anion Receptors. In *Encyclopedia of Supramolecular Chemistry*; Marcel Dekker: New York, NY, 2004; p 31; (c) Sukasai, C.; Tuntulani, T. *Chem. Soc. Rev.* **2003**, *32*, 192–202; (d) Gale, P. A. *Acc. Chem. Res.* **2006**, *39*, 465–475; (e) Martinez-Manez, R.; Sancenon, F. *Chem. Rev.* **2003**, *103*, 4419–4476; (f) De Silva, A. P.; Gunaratne, H. Q. N.; Gunnlaugsson, T.; Hauxley, A. J. M.; McCoy, C. P.; Rademacher, J. T.; Rice, T. E. *Chem. Rev.* **1997**, *97*, 1515–1566; (g) Beer, P. D.; Gale, P. A. *Angew. Chem., Int. Ed.* **2001**, *40*, 486–516; (h) Yoon, J.; Kim, S. K.; Singh, J.; Kim, K. S. *Chem. Soc. Rev.* **2006**, *35*, 355–360; (i) Gunnlaugsson, T.; Glynn, M.; Tocci, G. M.; Kruger, P. E.; Pfeffer, F. M. *Coord. Chem. Rev.* **2006**, *250*, 3094–3117.
4. (a) Gunnlaugsson, T.; Davis, A. P.; Hussey, G. M.; Tierney, J.; Glynn, M. *Org. Biomol. Chem.* **2004**, *2*, 1856–1863; (b) Pfeffer, F. M.; Seter, M.; Lewcenko, N.; Barnett, N. W. *Tetrahedron Lett.* **2006**, *47*, 5241–5244; (c) Lee, J. Y.; Cho, E. J.; Mukamel, S.; Nam, K. C. *J. Org. Chem.* **2004**, *69*, 943–950; (d) Xu, G.; Tarr, M. A. *Chem. Commun.* **2004**, 1050–1052;

(e) Wu, C.-Y.; Chen, M.-S.; Lin, C.-A.; Lin, S.-C.; Sun, S.-S. *Chem.—Eur. J.* **2006**, *12*, 2263–2269.
5. (a) Choi, K.; Hamilton, A. D. *Coord. Chem. Rev.* **2003**, *240*, 101–110; (b) Hartley, J. H.; James, T. D.; Ward, C. J. *J. Chem. Soc., Perkin Trans. 1* **2000**, 3155–3184; (c) Lee, C. H.; Lee, J. S.; Na, H. K.; Yoon, D. W.; Miyji, H.; Cho, W. S.; Sessler, J. L. *J. Org. Chem.* **2005**, *70*, 2067–2074; (d) Mizukami, S.; Nagano, T.; Urano, Y.; Odani, A.; Kikuchi, K. *J. Am. Chem. Soc.* **2002**, *124*, 3920–3925; (e) Otón, F.; Tárraga, A.; Velasco, M. D.; Espinosa, A.; Molina, P. *Chem. Commun.* **2004**, 1658–1659; (f) Anzenbacher, P., Jr.; Try, C. A.; Miyaji, H.; Jursíková, K.; Lynch, V. M.; Marquez, M.; Sessler, J. L. *J. Am. Chem. Soc.* **2000**, *122*, 10268–10272.
6. (a) Lu, H.; Xu, W.; Zhang, D.; Zhu, D. *Chem. Commun.* **2005**, 4777–4779; (b) Curiel, D.; Beer, P. D.; Cowley, A.; Sambrook, M. R.; Szemes, F. *Chem. Commun.* **2004**, 1162–1163; (c) Li, Z.-B.; Lin, J.; Zhang, H.-C.; Sabat, M.; Hyacinth, M.; Pu, L. *J. Org. Chem.* **2004**, *69*, 6284–6293; (d) Cho, E. J.; Moon, J. W.; Ko, S. W.; Lee, J. Y.; Kim, S. K.; Yoon, J.; Nam, K. C. *J. Am. Chem. Soc.* **2003**, *125*, 12376–12377; (e) Curiel, D.; Cowley, A.; Beer, P. D. *Chem. Commun.* **2005**, 236–238.
7. (a) Amendola, V.; Boiocchi, D.; Colasson, B.; Fabbrizzi, L. *Inorg. Chem.* **2006**, *45*, 6138–6147; (b) Amendola, V.; Esteban-goä mez, D.; Fabbrizzi, L.; Licchelli, M. *Acc. Chem. Res.* **2006**, *39*, 343–353; (c) Lin, Z.-H.; Ou, S.-J.; Duan, C.-Y.; Zhang, B.-G.; Bai, Z.-P. *Chem Commun.* **2006**, 624–626; (d) Gale, P. A. *Chem. Commun.* **2005**, 3761–3763; (e) Xu, S.; Chen, K. C.; Tian, H. *J. Mater. Chem.* **2005**, 2676–2680; (f) Boioccho, M.; Boca, D. L.; Gomez, D. E.; Fabbrizzi, L.; Licchelli, M.; Monzani, E. *Chem.—Eur. J.* **2005**, *11*, 3097–3104; (g) Evgeny, A. K.; DanPantos, G.; Reshetova, M. D.; Khrustalev, V. N.; Lynch, V. M.; Ustynyuk, Y. A.; Sessler, J. L. *Angew. Chem., Int. Ed.* **2005**, *44*, 7386–7390; (h) Nielsen, K. A.; Cho, W.-S.; Lyskawa, J.; Levillain, E.; Lynch, V. M.; Sessler, J. L.; Jeppesen, J. O. *J. Am. Chem. Soc.* **2006**, *128*, 2444–2451 and reference cited therein; (i) Peng, X.; Wu, Y.; Fan, J.; Tian, M.; Han, K. *J. Org. Chem.* **2005**, *70*, 10524–10531.
8. (a) Jose, D. A.; Kumar, D. K.; Ganguly, B.; Das, A. *Org. Lett.* **2004**, *6*, 3445–3448; (b) Jose, D. A.; Kumar, D. K.; Ganguly, B.; Das, A. *Tetrahedron Lett.* **2005**, *46*, 5343–5346; (c) Jose, D. A.; Singh, A.; Ganguly, B.; Das, A. *Tetrahedron Lett.* **2007**, *48*, 3695–3698; (d) Gomez, D. E.; Fabbrizi, L.; Licchelli, M.; Monzani, E. *Org. Biomol. Chem.* **2005**, *3*, 1495–1500; (e) Bordwell, F. G. *Acc. Chem. Res.* **1988**, *21*, 456–463; (f) Kwon, J. Y.; Singh, N. J.; Kim, H.; Kim, S. K.; Yoon, J. *J. Am. Chem. Soc.* **2004**, *126*, 8892–8893; (g) Kwon, J. Y.; Jang, Y. J.; Kim, S. K.; Lee, K.-H.; Kim, J. S.; Yoon, J. *J. Org. Chem.* **2004**, *69*, 5155–5157; (h) Kim, Y.-J.; Kwak, H.; Lee, S. J.; Lee, J. S.; Kwon, H. J.; Nam, S. H.; Lee, K.; Kim, C. *Tetrahedron* **2006**, *62*, 9635–9640; (i) Gunnlaugsson, T.; Davis, A. P.; O'Brien, J. E.; Glynn, M. *Org. Lett.* **2002**, *4*, 2449–2452.
9. (a) Boiocchi, M.; Boca, L. D.; Gomez, D. E.; Fabbrizzi, L.; Licchelli, M.; Monzani, E. *J. Am. Chem. Soc.* **2004**, *126*, 16507–16514; (b) Evans, L. S.; Gale, P. A.; Light, M. E.; Quesada, R. *Chem. Commun.* **2006**, 965–967; (c) Ghosh, T.; Maiya, B. G.; Wong, M. W. *J. Phys. Chem. A* **2004**, *108*, 11249–11259.
10. (a) TITAN; Wavefunction, Inc., 18401 Von Karman Avenue, Suite 370, Irvine, CA 92612, USA, Schrodinger, Inc., 1500 SW First Avenue, Suite 1180, Portland, OR 97201, USA; (b) The interaction energy is obtained by the energy of the complex subtracted from the sum of the constituent energies. The interaction is very strong due to charged hydrogen bonds. Thus, the basis set superposition error (BSSE) is expected to be negligible compared to the magnitude of the total interaction energies.
11. One can find further support from the fact that there should be higher overlap in the red shifted absorption band for the naphthalene unit adjacent to the deprotonated urea derivative and the emission band for the nitrobenzene unit as compared to that of the corresponding urea derivative before deprotonation.
12. (a) Inoue, H.; Hida, M.; Nakashima, N.; Yoshihara, K. *J. Phys. Chem.* **1982**, *86*, 3184–3188; (b) Yatsuhashi, T.; Nakajima, Y.; Shimada, T.; Inoue, H. *J. Phys. Chem. A* **1998**, *102*, 3018–3024.
13. *SAINT+, 6.02 ed*; Bruker AXS: Madison, WI, 1999.
14. (a) Sheldrick, M. *SHELXTL Reference Manual, Version 5.1*; Bruker AXS: Madison, WI, 1997; (b) Sheldrick, G. M. *SHELXL–97: Program for Crystal Structure Refinement*; University of Göttingen: Göttingen, Germany, 1997.
15. Mercury 1.4.1 Supplied with Cambridge Structural Database, Copyright CCDC, 2005–2006.
16. Perisamy, N.; Doraiswamy, S.; Maiya, G. B.; Venkataraman, B. *J. Chem. Phys.* **1988**, *88*, 1638–1651.
17. Bevington, P. R. *Data Reduction and Error Analysis for the Physical Sciences*; McGraw-Hill: New York, NY, 1969.